

## Research



**Cite this article:** Hui C-Y, Cui F, Zehnder A, Vernerey FJ. 2021 Physically motivated models of polymer networks with dynamic cross-links: comparative study and future outlook. *Proc. R. Soc. A* **477**: 20210608.  
<https://doi.org/10.1098/rspa.2021.0608>

Received: 27 July 2021

Accepted: 15 October 2021

**Subject Areas:**

mechanical engineering, mathematical modelling, mechanics

**Keywords:**

transient networks, polymer, viscoelasticity, constitutive modelling

**Author for correspondence:**

Franck J. Vernerey

e-mail: [franck.vernerey@colorado.edu](mailto:franck.vernerey@colorado.edu)

Chung-Yuen Hui and Franck J. Vernerey contributed equally to this work as first authors.

Electronic supplementary material is available online at <https://doi.org/10.6084/m9.figshare.c.5702508>.

# Physically motivated models of polymer networks with dynamic cross-links: comparative study and future outlook

Chung-Yuen Hui<sup>1</sup>, Fan Cui<sup>1</sup>, Alan Zehnder<sup>1</sup> and Franck J. Vernerey<sup>2</sup>

<sup>1</sup>Field of Theoretical and Applied Mechanics, Department of Mechanical and Aerospace Engineering, Cornell University Ithaca, Ithaca, NY14853, USA

<sup>2</sup>Department of Mechanical Engineering, University of Colorado Boulder, Boulder, CO 80309, USA

C-YH, 0000-0001-7270-6000; FJV, 0000-0001-6138-1431

Polymer networks consisting of a mixture of chemical and physical cross-links are known to exhibit complex time-dependent behaviour due to the kinetics of bond association and dissociation. In this article, we highlight and compare two recent physically based constitutive models that describe the nonlinear viscoelastic behaviour of such transient networks. These two models are developed independently by two groups of researchers using different mathematical formulations. Here, we show that this difference can be attributed to different viewpoints: Lagrangian versus Eulerian. We establish the equivalence of the two models under the special situation where chains obey Gaussian statistics and steady-state bond dynamics. We provide experimental data demonstrating that both models can accurately predict the time-dependent uniaxial behaviour of a poly(vinylalcohol) dual cross-link hydrogel. We review the advantages and disadvantages of both approaches in applications and close by discussing a list of open challenges and questions regarding the mathematical modelling of soft, viscoelastic networks.

## 1. Introduction

In recent years, advances in synthetic chemistry have unlocked the potential for an enormous variety of

polymers with diverse molecular architectures and cross-linking types. In particular, the incorporation of physical or non-covalent bonds have enabled the fabrication of networks that display high toughness [1–3], self-healing capabilities [4–6] and recyclability. An ever-expanding library of non-permanent and reversible bonds can now be created with high control, that can generally be classified in three families: physical bonds, adaptable covalent bonds and topological bonds. Physical bonds, such as hydrogen bonding, ionic bonding,  $\pi$ - $\pi$  and host-guest interactions acquire their reversible nature from their inherently lower activation energy. In this case, the presence of thermal noise increases the probability of bond breaking and reformation, implying that the chain association/dissociation increase with temperature. By contrast, bond dynamics in covalent adaptable networks is activated by a stimulus (which may be triggered by a catalyst, light or a change of temperature) and may thus be turned on and off externally. Experimentally, networks often combine a mixture of permanent bonds formed by covalent cross-links and dynamic bonds. This is the case of the poly(vinylalcohol) (PVA) gels considered in this work, or other systems, such as discussed in [1] where a dual cross-link PVA hydrogel consists of glutaraldehyde chemical cross-linkers mixed with borate ions providing reversible bonds. In fact, the reversible nature of the physical bond, together with the way they are organized, contribute significantly to mechanical properties such as viscoelasticity, damage, fracture and self-healing of the networks. This micro-macro connection is often difficult to quantify, and this is rendered even more challenging with the increasing complexity of network that can either be fabricated in laboratories or found in natural materials. To overcome this obstacle, theoretical approaches must provide a link between the molecular structure, the physical mechanisms at play and the emerging response of the network.

More specifically, an important challenge in modelling soft viscoelastic materials is that they uniquely combine flow properties, exhibited by viscous fluids, with large strain elasticity that characterizes solids. They are, therefore, able to flow and change the reference configuration over a long time, while storing significant elastic energy over short time scales. From a modelling viewpoint, they, therefore, fall at the boundary of solid and fluid mechanics. Therefore, it is not surprising that, historically, attempts to describe these materials have taken two distinct approaches. The Lagrangian approach, traditionally taken by solid mechanicians, relies on the definition of a reference configuration, about which all subsequent measures of deformation are taken. By contrast, the Eulerian approach, preferred by fluid mechanicians, does not consider an absolute reference for the deformation, but rather updates this reference over time. Fundamentally, these two schools of thought originate from the physical idea that solids have an infinite memory of their deformation history, while fluids have no memory at all. Since viscoelastic materials do have a memory that fades over time, it is not clear which of the two approaches should be taken. An example of the Lagrangian approach to modelling soft material viscoelasticity is illustrated by the recent work of Mao *et al.* [2]. In [2], the deformation gradient is multiplicatively decomposed into an elastic and a viscous part. The key ingredient in this treatment is the use of state variables to track the microstructural changes in the networks and the introduction of a flow rule that determines the evolution of the viscous deformation gradient. Examples of the Eulerian approach include the upper-convected Maxwell model [3] and the Oldroyd-B model [4], which describe the flow of viscoelastic fluids. Finally, mixed Lagrangian and Eulerian approaches are used by the complex fluid community, where the emphasis is on behaviours such as shear thinning/thickening and transitions between solid-like and fluid-like behaviour. Here, the material may alternatively be interpreted as an elastic fluid, whose rheological behaviour combines flow and elastic deformation.

In this work, we focus on physically based constitutive models for soft viscoelastic solids that connect the details of the network dynamics and the individual chain response. A schematic view of an ideal flexible dynamic network, with rates of association and dissociation  $\xi_a$  and  $\xi_d$ , respectively, is presented in figure 1. Two main directions have, recently, been taken. The first, introduced by Long *et al.* [5] and Guo *et al.* [6], considers population of polymer chains born at different times. Their relative contribution to the mechanics of the network, therefore, depends on two factors: the deformation from the time they were born and the rate at which they

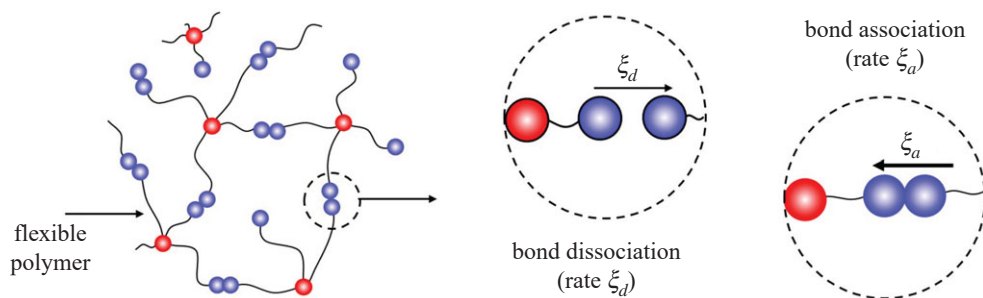


**Figure 1.** Illustration of a transient polymer network, showing the association of dangling chains at average rate  $\xi_a$  and dissociation of previously connected chains at average rate  $\xi_d$ . Red spheres represent permanent cross-links. (Online version in colour.)

dissociate from the network. Because of this, the mathematical formulation relies on a history integral that keeps track of both the deformation path and the network dynamic over time (see equation (2.4a)). The second approach, also known as the transient network theory (TNT) [7–9], is based on a statistical description of the chain population in the network, in terms of a distribution function where the independent variables are the end-to-end vector  $r$  (or conformation) of chains in the network and time. With this view, each material point is endowed with a three-dimensional space of conformation  $\Omega$ , spanned by the end-to-end vectors of the underlying network. Using concepts of statistical mechanics, this theory introduces an evolution equation for the distribution function, known as the Fokker–Planck equation that is driven by both the deformation history and the rates of chain association and dissociation. Knowledge of the distribution function enables a reconstruction of the stored elastic energy, viscous dissipation and network stress. Thus, although these formulations are both deeply anchored to a physical description of the underlying network, they take very distinct mathematical forms that have their own advantages and limitations depending on the practical problem at hand.

The objective of this work is, therefore, to provide a summary and discussion of these two approaches, including their differences and similarities, as well as their respective limitations and potentials. Notably, we show that the key distinction between these approaches originates from the dual Lagrangian/Eulerian point of view when describing the motion of chains in their conformation space. Thus, the integral approach may be thought of as the Lagrangian, solid mechanics approach to dynamic networks, while the TNT belongs to the Eulerian, fluid mechanics alternative. This dual viewpoint naturally follows from the fact that transient networks do exhibit a dual behaviour, often characterized by elasticity at short time scales and viscosity at long time scales. The manuscript is organized as follows. Section 2 starts by providing a synthetic description of the Lagrangian and Eulerian approaches. Since these two approaches are independently obtained, we retain the notations for physical quantities used in the original works. In §3, we will establish equivalence between key physical quantities in both approaches. More specifically, §3 compares the two approaches and identifies conditions in which the approaches converge to the same solutions. These solutions are further illustrated by fitting the time-dependent response of a dynamic, dual network hydrogel (PVA). Section 4 finally assesses the advantages and disadvantages of each approach and discusses their potential in addressing a number of open questions in the emerging field of dynamic and supramolecular polymer networks.

## 2. Physically informed formulations for transient network

We here concentrate on providing a continuum description of a polymer network made of flexible chains that can associate and dissociate from the rest of the network over time (figure 1). A given polymer chain may, therefore, be found in two states. The first corresponds to that of an

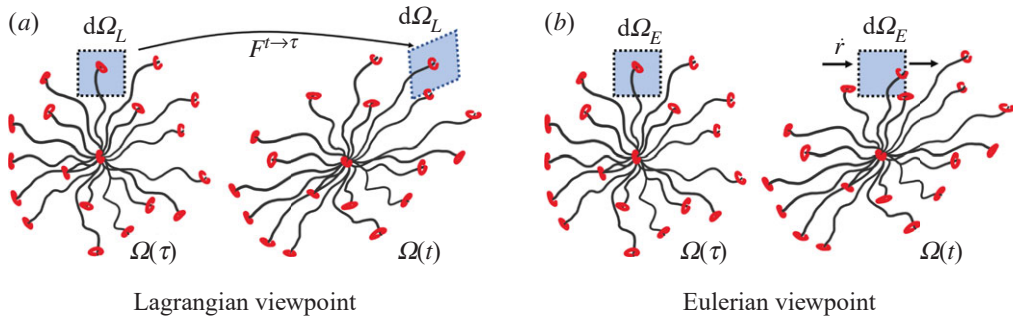


**Figure 2.** Schematic representation of the conformation space embedded in a material point. A given chain conformation is here shown by a chain that changes its end-to-end vector as the material volume is subjected to deformation, or when bond dynamics is activated. (a) In the Lagrangian view, we follow the motion of a population of chains (all born at a given time  $\tau$ ), as indicated by the motion of the Lagrangian window  $d\Omega_L$ . (b) In the Eulerian view, we monitor the change in chain density  $\phi(\mathbf{r}, t)$  in a fixed Eulerian window  $d\Omega_E$ . (Online version in colour.)

‘effective chain’ (which is equivalent to the active chains in the terminology used by Tanaka & Edwards [10]) that is attached to the network at both of its ends, and, therefore, is a load bearing element. The second is a dangling state, where the chain is not connected to the network and, therefore, does not participate in its mechanical integrity. For simplicity, we assume that the bond exchange reaction is independent of deformation and is, therefore, found in a steady-state where the rate of attachment is equal to the rate of detachment ( $\xi_a = \xi_d$ ). Let us consider that the network embedded at a material point is deformed according to a general, time-dependent deformation gradient  $F(t)$ . The corresponding velocity gradient (that expresses the rate of deformation) is then given by

$$L = \dot{F}F^{-1}, \quad (2.1)$$

where a dot denotes differentiation with time. Assuming instantaneous affine deformation, the time rate of change of a connected chain’s end-to-end vector  $\mathbf{r}$  is

$$\dot{\mathbf{r}} = L\mathbf{r}. \quad (2.2)$$

To characterize the mechanical response of the network over time, we seek to compute the strain energy density of the physical chains in the dynamic network at the current time  $t$  for a given deformation history, characterized by the deformation gradient  $F(\tau)$ ,  $\tau \in (-\infty, t)$ . For this purpose, it is convenient to visually represent the deformation of chains in the network via their end-to-end vectors  $\mathbf{r}$  over time (figure 2). To follow the history of the network deformation, two distinct viewpoints may be taken. As depicted in figure 2, the Lagrangian viewpoint follows the motion of a specific subpopulation of chains embedded in a small Lagrangian window  $d\Omega_L$  over time. By contrast, the Eulerian viewpoint considers a fixed window  $d\Omega_E$  in the space of conformation and assesses the change in chain density at this point. We show below that these dual points of view lead to distinct, yet complementary formulations to describe transient networks.

### (a) The Lagrangian formulation

In this section, we summarize the continuum approach in [1,2]. Here, the observer follows the density and deformation of a population of effective chains that are born (i.e. that are associated with the network) within a small time interval between  $\tau$  and  $\tau + d\tau$ . For this purpose, we denote the number of effective chains per unit reference volume that are born between time  $\tau$ ,  $\tau + d\tau$  and survive to  $t$  by  $n(t, \tau)d\tau$  (figure 3a).

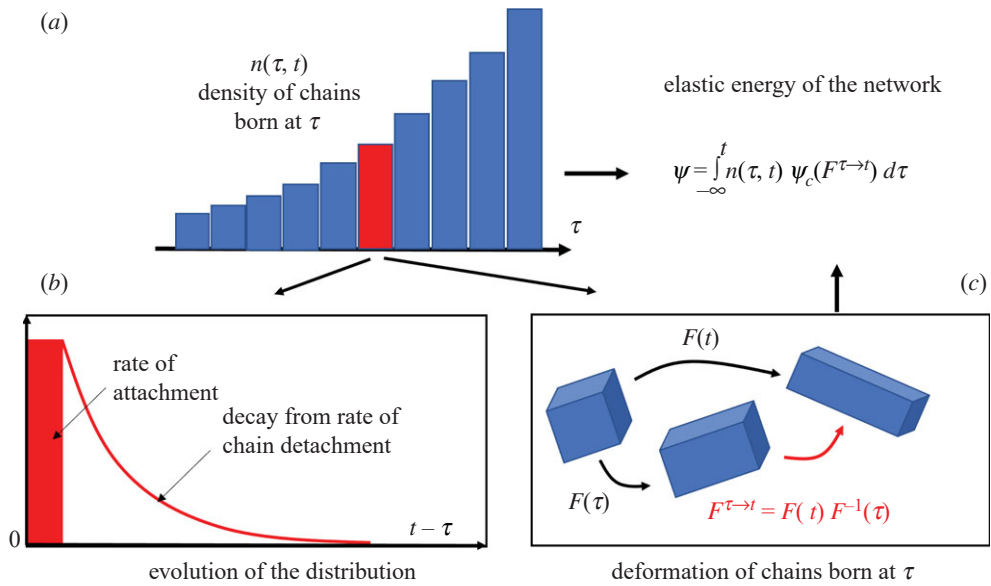


**Figure 3.** Illustration of the Lagrangian point of view. Here, the physical state of a material point is described by a distribution of subnetworks born at time  $\tau$ . Each of these networks is characterized by its chain concentration  $n(\tau, t)$  and deformation  $F^{\tau \rightarrow t}$ , which is measured between times  $\tau$  and  $t$  (a,c). It is possible to evaluate the change in concentration over time by the knowledge of the rate of attachment (setting the chain concentration  $n(\tau, \tau)$  of the network at the initial time) and the rate of detachment (which triggers a decay of the concentration  $n(\tau, t)$  over time, b). The elastic energy of the full network is then found as the weighted summation of the stored energies  $\psi_c(F^{\tau \rightarrow t})$  in each subnetwork (shown by an integral in (a)). (Online version in colour.)

### (i) Strain energy function

Let us now estimate the elastic energy stored in the subpopulation of chains  $n(t, \tau)d\tau$  (represented by the red histogram in figure 3a). The deformation experienced by this subpopulation is given by the ‘partial’ deformation gradient

$$F^{\tau \rightarrow t} = F(t)F^{-1}(\tau), \quad (2.3a)$$

where the subscript  $\tau \rightarrow t$  indicates that the physical chain experiences the deformation history from its birth (reattachment) at  $\tau$  to the current time  $t$ . Assuming that effective chains are born in a deformation-free state, that is,  $F^{\tau \rightarrow \tau} = \mathbf{I}$  at birth, with  $\mathbf{I}$  the identity tensor. If we now assume that the elastic energy of a single chain is  $\psi_c$ , the contribution from this subpopulation of chains to the total stored energy per unit reference volume is

$$n(t, \tau)\psi_c(F^{\tau \rightarrow t})d\tau. \quad (2.3b)$$

If the bond exchange rate is independent of deformation, the chain dynamics remain in a steady state where the rate of association becomes equal to the rate of dissociation. If we denote this rate by  $\gamma_\infty$  (number of chains per unit reference volume that are born/destroyed per unit time), then  $n(t, \tau)$  can be expressed as

$$n(t, \tau) = \gamma_\infty \phi_B(t, \tau), \quad (2.4)$$

where  $\phi_B(t, \tau)$  is the fraction of chains that are born at  $\tau$  and survive at  $t$ . Here, we note that  $\phi_B(t = \tau, \tau) = 1$ , which implies that  $n(t = \tau, \tau) = \gamma_\infty$ . The steady-state assumption implies that  $\phi_B(t, \tau)$  is time translation invariant, that is,  $\phi_B(t, \tau) = \phi_B(t - \tau)$ .

If the polymer is made of the combination of this dynamic network and a permanent network with  $n_p$  chains per unit reference volume, then the total strain energy is the sum of the strain

energies carried by (i) the permanent chains and (ii) the cumulation of chains (from the dynamic network) born at all times. The strain energy density per unit reference volume thus becomes:

$$\Psi = n_p \psi_c(\mathbf{F}(t)) + \int_{-\infty}^t \gamma_{\infty} \phi_B(t - \tau) \psi_c(\mathbf{F}^{\tau \rightarrow t}) d\tau, \quad (2.5a)$$

where we have assumed the same strain energy model applies to effective chains in the permanent and dynamic network. Furthermore, defining  $N_{ss}$  as the number of connected chains per unit reference volume, we can introduce  $\bar{\gamma}_{\infty} = \gamma_{\infty}/N_{ss}$ ,  $\rho_p = n_p/N_{ss}$ , so that  $\bar{\gamma}_{\infty}$  is the molar fraction of chains per unit reference volume that are born per unit time and  $\rho_p$  is the molar fraction of permanent chains per unit reference volume. With this new notation, equation (2.5a) becomes:

$$\Psi = \rho_p W(\mathbf{F}(t)) + \int_{-\infty}^t \bar{\gamma}_{\infty} \phi_B(t - \tau) W(\mathbf{F}^{\tau \rightarrow t}) d\tau, \quad (2.5b)$$

where  $W(\mathbf{F}) = N_{ss} \psi_c(\mathbf{F})$  is identified as the continuum strain energy density function for the network.

### (ii) Kinetics of bond exchange and steady-state concentrations

The kinetic model for breaking is

$$\frac{d(n(t, \tau)/n(\tau, \tau))}{dt} = \frac{-(n(t, \tau)/n(\tau, \tau))^{\alpha_B}}{t_B}, \quad (2.6)$$

where  $t_B$  is a characteristic time constant for breaking (figure 1) and  $\alpha_B$  is a material parameter that describes the spectrum of relaxation times of the dynamic network. Integrating equation (2.6) leads to:

$$n(t, \tau) = \gamma_{\infty} [1 - (1 - \alpha_B)(t - \tau)/t_B]^{1/(1 - \alpha_B)}, \quad (2.7)$$

where we have enforced the initial condition  $n(t = \tau, \tau) = \gamma_{\infty}$ . The molar fraction of connected chains in the dynamic network,  $\rho_c = n_c/N_{ss}$  then becomes:

$$\rho_c = \frac{1}{N_{ss}} \int_{-\infty}^t n(t, \tau) d\tau = \int_{-\infty}^t \bar{\gamma}_{\infty} [1 - (1 - \alpha_B)(t - \tau)/t_B]^{1/(1 - \alpha_B)} d\tau = \frac{\bar{\gamma}_{\infty} t_B}{2 - \alpha_B}. \quad (2.8)$$

In this model, the association rate is directly proportional to the number of detached physical chains per unit reference volume  $n_d$  divided by the characteristic healing time  $t_H$ . At steady state, the association rate  $n_d/t_H$  is constant and

$$n_d/t_H = \gamma_{\infty}. \quad (2.9)$$

The steady-state healing rate  $\bar{\gamma}_{\infty} \equiv \gamma_{\infty}/N_{ss}$  can be determined by noting that the total fraction of physical bonds is  $1 - \rho_p$ . Using equations (2.8) and (2.9),

$$\frac{n_c + n_d}{N_{ss}} = \frac{\bar{\gamma}_{\infty} t_B}{2 - \alpha_B} + \bar{\gamma}_{\infty} t_H = \bar{\gamma}_{\infty} \left[ \frac{t_B}{2 - \alpha_B} + t_H \right] = 1 - \rho_p \Rightarrow \bar{\gamma}_{\infty} = \frac{1 - \rho_p}{\frac{t_B}{2 - \alpha_B} + t_H}. \quad (2.10)$$

### (iii) Stress-deformation relation

To enforce incompressibility, the energy density  $\Psi$  is modified to include an additional term  $-p[\det(\mathbf{F}(t)) - 1]$ , where  $p$  is a Lagrange multiplier. This results in the true stress given by Mao *et al.* [2]

$$\boldsymbol{\sigma} = -p\mathbf{I} + \rho_p \frac{\partial W}{\partial \mathbf{F}} \mathbf{F}^T + \left[ \int_{-\infty}^t \bar{\gamma}_{\infty} \phi_B(t - \tau) \frac{\partial W}{\partial \mathbf{F}} \Big|_{\mathbf{F}=\mathbf{F}^{\tau \rightarrow t}} \mathbf{F}^{-T} d\tau \right] \mathbf{F}^T. \quad (2.11)$$

In the following, we assume a neo-Hookean network where

$$W = \frac{G}{2} (\text{tr}(\mathbf{F}^T \mathbf{F}) - 3) \Rightarrow \frac{\partial W}{\partial \mathbf{F}} \Big|_{\mathbf{F}=\mathbf{F}^{\tau \rightarrow t}} = G \mathbf{F}^{\tau \rightarrow t} \quad (2.12a)$$

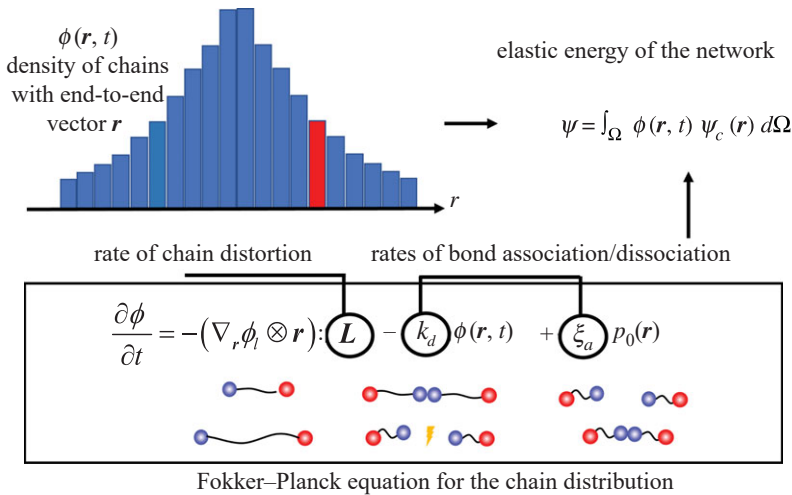


**Figure 4.** Illustration of the Eulerian point of view. Here, the physical state of a material point is described by the distribution  $\phi(\mathbf{r}, t)$  of the end-to-end vector  $\mathbf{r}$  of the chains in the polymer network. In this approach, we do not follow the deformation of each chain over time, but rather follow the evolution of the full distribution through the Fokker–Planck equation that comprises three terms: a distortion term that arises from the affine deformation of chain under the action of the overall velocity gradient  $\mathbf{L} = \dot{\mathbf{F}}\mathbf{F}^{-1}$ , a sink term that arises from the rate of chain dissociation and a source term that arises from the rate of chain association. As in the Lagrangian approach, the elastic energy of the full network can then be reconstructed as the weighted summation of the stored energies  $\psi_c(\mathbf{r})$  in chains with different conformations. (Online version in colour.)

where  $G$  is the small strain modulus. Assume loading starts at  $t \geq 0$ , so  $\mathbf{F}(t \leq 0) = \mathbf{I}$  and using equation (2.12a), equation (2.11) simplifies to:

$$\boldsymbol{\sigma}(t \geq 0) = G[\rho_p + \bar{n}(t)]\mathbf{F}(t)\mathbf{F}^T(t) + \left[ G\bar{\gamma}_\infty \mathbf{F}(t) \int_0^t \phi_B(t - \tau)\mathbf{F}^{-1}(\tau)\mathbf{F}^{-T}(\tau)d\tau \right] \mathbf{F}^T(t) - p\mathbf{I}, \quad (2.12b)$$

where

$$\bar{n}(t) \equiv \bar{\gamma}_\infty \int_t^\infty \phi_B(\tau)d\tau = \frac{\bar{\gamma}_\infty t_B}{2 - \alpha_B} [1 + (\alpha_B - 1)t/t_B]^{(2 - \alpha_B)/(1 - \alpha_B)}. \quad (2.12c)$$

We note here that equation (2.12b) is the true stress given in Long *et al.* [5].

## (b) The Eulerian formulation

In the statistical mechanics formulation described by Vernerey *et al.* [9], the full network is first divided into several subnetworks ( $l = 1, N$ ), each possessing their own bond exchange reaction rate. For clarity of the exposition, let us concentrate on one of these networks (say the  $l$ th network). In contrast to the above Lagrangian approach, the description of the network follows here the Eulerian view, where an observer remains fixated on a particular conformation of a polymer chain, characterized by its end-to-end vector  $\mathbf{r}$  (figure 4). Since this variable is continuous, we concentrate here on the number of effective chains per reference volume, with conformation  $\mathbf{r}$  as shown in figure 4. The number  $dN$  of effective chains that belong to  $l$ th network is represented by

$$dN = \phi_l(\mathbf{r}, t)d\Omega, \quad (2.13a)$$

where the function  $\phi_l$  is the end-to-end vector distribution and  $d\Omega = r^2 \sin\theta dr d\theta d\omega$  is an infinitesimal element of the conformation space  $\Omega$ . This chain distribution function  $\phi_l(\mathbf{r}, t)$ , therefore, characterizes the density of chains whose end-to-end distance is between  $r$  and  $r + dr$  and orientation is between  $(\theta, \omega)$  and  $(\theta + d\theta, \omega + d\omega)$ .

The chain distribution function can further be multiplicatively decomposed in terms of the chain concentration  $c_l(t)$  and the probability density function  $P_l(\mathbf{r}, t)$  according to

$\phi_l(r, t) = c_l(t)P_l(r, t)$ . Here,  $c_l(t)$  is the number of connected chains (in moles) in the  $l$ th network per unit reference volume and  $P$  is the probability density of finding a chain with end-to-end vector  $r$  at time  $t$ , that satisfies:

$$\int_{\Omega} P_l(r, t) d\Omega = 1, \quad \text{where} \quad \int_{\Omega} [\cdot] E \Omega \equiv \int_0^{2\pi} d\omega \int_0^{\pi} \sin\theta d\theta \int_0^{\infty} [\cdot] r^2 dr. \quad (2.13b)$$

Therefore, in the most general case, the  $l$ th network is statistically described by either  $\phi_l(r, t)$  or the two functions  $c_l(t)$ ,  $P_l(r, t)$ ,

### (i) Strain energy function

Consider a population of chains  $\phi_l(r, t) d\Omega$ , the stored elastic energy per unit current volume for this chain population is  $\phi_l(r, t) \psi_c(r) d\Omega$ , where  $\psi_c(r)$  is the elastic energy stored in a single chain. The total stored elastic energy per unit current volume,  $\Psi_l$  is obtained by integration over all of chain space

$$\Psi_l \equiv \int_{\Omega} \phi_l(r, t) \psi_c(r) d\Omega. \quad (2.14a)$$

For Gaussian chains,

$$\psi_c(r) = \frac{3k_B T}{2Nb^2} r^2 \phi_l(r, t=0) = c_l(t=0) \left( \frac{3}{2\pi N_l b_l^2} \right)^{3/2} \exp\left(-\frac{3|r|^2}{2N_l b_l^2}\right), \quad (2.14b,c)$$

where  $k_B$  is the Boltzmann's constant,  $T$  is the absolute temperature,  $N_l$  is the number of Kuhn segments and  $b_l$  is the Kuhn length of a chain in the  $l$ th network. Using equations (2.14b,c), it has been shown that the energy stored in the  $l$ th network, equation (2.14a) takes the simple expression [9]:

$$\Psi_l = \frac{c_l k_B T}{2} \text{Tr}(\mu_l), \quad (2.14d)$$

where  $\mu_l$  is the conformation tensor (associated with the  $l$ th network), defined as

$$\mu_l = \frac{3}{Nb^2} \int_{\Omega} P_l(r, t) r \otimes r d\Omega, \quad (2.15)$$

with  $\otimes$  the dyadic product. This symmetric tensor represents the mean square stretch of the chains in the network, along with the principal direction of stretch. It can be verified that  $\mu_l = \mathbf{I}$  when the network is stress-free. The energy in the full network  $\Psi$  can finally be written as the sum of the contribution from each subnetwork

$$\Psi = \sum_l \Psi_l - p[\det(\mathbf{F}(t)) - 1], \quad (2.16)$$

where the term  $-p[\det(\mathbf{F}(t)) - 1]$  is added to enforce incompressibility.

### (ii) Kinetics of bond exchange and steady-state concentrations

To close the model, it is now necessary to specify how chains break and reattach. For this purpose, let us assume that effective chains attach to the network at an average rate  $\xi_a^l$  (units moles/time) and detach at an average rate  $\xi_d^l = k_d^l c^l$ , where  $c^l$  is the molar concentration of effective chains in the  $l$ th network and  $k_d^l$  is the kinetic coefficient describing their dissociation. We have previously shown in [9] that under these conditions, the time evolution of the chain distribution is given by the Fokker–Planck equation (see figure 4 for illustration):

$$\frac{\partial \phi_l}{\partial t} = -(\nabla_r \phi_l \otimes r) : L + \xi_a^l p_0(r) - k_d^l(r) \phi_l, \quad (2.17)$$

where  $' :$ ' denotes the double tensor contraction and  $p_0(r)$  is the probability density function at which newly born chains attach to the network. It is usually defined by an isotropic multivariate Gaussian with zero mean and a covariance of  $(\sqrt{N_l} b_l / 3) \mathbf{I}$ .

### (iii) Stress-deformation relation

Consider a polymer consisting of a permanent network with concentration  $c_p$  (no. chains per unit current volume) and multiple non-interacting dynamic networks indexed by  $l = 1, \dots, M$ ; each has their own chain concentration  $c_l(t)$  and distribution  $\phi_l$  (or alternatively, conformation tensor  $\mu_l$ ). Using the Coleman–Knoll procedure, it can be shown that the true stress  $\sigma$  is given by

$$\sigma = -p\mathbf{I} + \sum_l \int_{\Omega} \phi_l(\mathbf{r}, t) \nabla_{\mathbf{r}} \psi_l \otimes \mathbf{r} d\Omega. \quad (2.18)$$

### (c) The reduced transient network theory

We have seen in equations (2.14d) and (2.15) that when the chain is Gaussian, the physical state of the network is fully described by the two time-dependent quantities  $c_l$  and  $\mu_l$ . In this situation, the governing equation of the TNT can be significantly simplified by describing the network statistics in terms of the conformation tensor  $\mu_l$  (in addition to the chain concentration  $c_l(t)$ ), rather than the full distribution  $\phi_l(\mathbf{r}, t)$ . The key difference between the fully developed and the reduced form of the theory is, therefore, with regard to the amount of information required to describe the state of a network. A consequence is that the reduced formulation does not require an integration over the full configuration space  $\Omega$  (assuming the conformation tensor  $\mu_l$  is known) to compute the stored elastic energy in equation (2.14d), representing a significant simplification compared with equation (2.14a). In addition to Gaussian chains, the reduced TNT (or RTNT) also requires that the rate of chain detachment  $k_d^l$  is independent of  $\mathbf{r}$ . For this case, the partial differential equation (2.17) can be replaced by two ordinary differential equations: one for the concentration  $c_l$  and one for the conformation tensor  $\mu_l$ , respectively [1]<sup>1</sup>. They are

$$\dot{c}_l = -k_d^l c_l + k_a(c_l^t - c_l) \quad (2.19a)$$

and

$$\dot{\mu}_l = \frac{\xi_a^l}{c_l} \mathbf{I} - k_d^l \mu_l - \frac{\dot{c}_l}{c_l} \mu_l + \mathbf{L}\mu_l + (\mathbf{L}\mu_l)^T, \quad (2.19b)$$

where  $c_l^t$  and  $c_l(t)$  are the total and effective molar concentration of chains, respectively. In equation (2.19a), we have used first-order kinetic models of the form  $\xi_a^l = k_a^l c_l$  and  $\xi_d = k_a(c_l^t - c_l)$ , for the dissociation and association of effective chains, respectively. We note here that since the kinetic constants  $k_d^l$  and  $k_a$  do not depend on deformation, each network quickly reaches their steady-state rate of association/dissociation  $\xi_a^l = \xi_d^l = k_d^l c_l^*$  where  $c_l^*$  is the steady state concentration of effective chains for the  $l$ th network. Therefore, at steady state, equations (2.19a,b) can be replaced by a single evolution equation for the conformation tensor:

$$\dot{\mu}_l = k_d^l (\mathbf{I} - \mu_l) + \mathbf{L}\mu_l + (\mathbf{L}\mu_l)^T. \quad (2.20)$$

When the elastic energy for a polymer chain is Gaussian, its derivative with respect to  $\mathbf{r}$  becomes linear, and the stress takes the simple form (RTNT):

$$\sigma = k_B T \sum_l c_l(t) (\mu_l - \mathbf{I}) - p\mathbf{I}. \quad (2.21)$$

In steady state, the total chain distribution tensor is a weighted sum of the contribution  $\mu_l$  from each network as

$$\boldsymbol{\mu} = \frac{c_p}{c^*} \boldsymbol{\mu}_p + \sum_{l=1}^M \frac{c_l^*}{c^*} \boldsymbol{\mu}_l, \quad (2.22a)$$

<sup>1</sup> $D$ , the symmetric part of  $L$  in [1] should be  $L$ .

where  $\mu_p = F(t)F^T(t)$  is associated with the permanent elastic network (with covalent cross-links) and the total steady-state chain concentration is

$$c^* = c_p + \sum_{l=1}^M c_l^* \quad (2.22b)$$

For this case, equation (2.21) simplifies to

$$\sigma = k_B T c^* (\mu - I) - p I \quad (2.22c)$$

### 3. Model comparison and experimental interpretation

The difference of viewpoint between the two models gives rise to notable contrasts in their mathematical formulations. The stress formula in the Lagrangian approach relies on a convolution time integral, that spans the time elapsed from the initial to the current time. It may, therefore, be cast as an integral formulation (see equation (2.11)). By contrast, the stress calculation with the Eulerian approach involves the solution of a differential equation for the conformation tensor, which classifies the approach as differential (see equation (2.17) for TNT). To compare the two models, we first highlight their equivalence in the special case of Gaussian (linear) chain response and linear bond kinetics (RTNT).

#### (a) Model equivalence for linear chain kinetics

To compare the two models, let us seek a general solution of the differential equation of the Eulerian approach for steady-state concentrations. For this, we first find that the solution of equation (2.20) that satisfies the initial condition  $\mu_l(t=0) = I$ ,  $F(t=0) = I$  is (see electronic supplementary material):

$$\mu_l = e^{-k_d^l t} F(t)F^T(t) + F(t) \left[ \int_0^t k_d^l e^{-k_d^l(t-\tau)} F^{-1}(\tau)F^{-T}(\tau) d\tau \right] F^T(t) \quad (3.1)$$

Substituting (3.1) in the stress expression (2.21c), the stress is (see electronic supplementary material):

$$\sigma = c^* k_B T \left[ \left( \frac{c_p}{c^*} + \sum_{l=1}^M \frac{c_l^*}{c^*} e^{-k_d^l t} \right) F(t)F^T(t) + F(t) \left[ \sum_{l=1}^M \frac{c_l^*}{c^*} \int_0^t k_d^l e^{-k_d^l(t-\tau)} F^{-1}(\tau)F^{-T}(\tau) d\tau \right] F^T(t) \right] - p I \quad (3.2)$$

where a constant term is absorbed in the Lagrange multiplier  $p$ . Next, we derive an equivalent model with the Lagrangian approach, let us assume that the dynamic network consists of  $M$  non-interacting subnetworks indexed by  $l = 1, \dots, M$ , each with their own concentrations  $n_l(t, \tau)$  and  $\bar{\gamma}_\infty^l$ . If a linear breaking kinetic model is considered, equation (2.6) is replaced by

$$\frac{dn_l(t, \tau)}{dt} = \frac{n_l(t, \tau)}{t_B^l} \Rightarrow n_l(t, \tau) = \bar{\gamma}_\infty^l e^{-(t-\tau)/t_B^l}, \quad (3.3)$$

where  $t_B^l$  is the characteristic breaking time constant for the  $l$ th network. For this case,  $\bar{\gamma}_\infty \phi_B(t - \tau)$  in equation (2.5b) and equation (2.12b) is replaced by  $\sum_{l=1}^M \bar{\gamma}_\infty^l e^{-(t-\tau)/t_B^l}$  and the true stress becomes (see electronic supplementary material):

$$\begin{aligned} \sigma(t \geq 0) = & G \left[ \rho_p + \sum_{l=1}^M \bar{\gamma}_\infty^l t_B^l e^{-t/t_B^l} \right] F(t)F^T(t) \\ & + GF(t) \left[ \sum_{l=1}^M \int_0^t \bar{\gamma}_\infty^l e^{-(t-\tau)/t_B^l} F^{-1}(\tau)F^{-T}(\tau) d\tau \right] F^T(t) - p I. \end{aligned} \quad (3.4)$$

Comparing equations (3.2) and (3.4), we find that the two models are in total agreement if we make the following associations between physical quantities:

$$c^*k_B T \leftrightarrow G, \quad \frac{c_p}{c^*} \leftrightarrow \rho_p, \quad \frac{c_l^*}{c^*} k_d^l \leftrightarrow \bar{\gamma}_\infty^l, \quad k_d^l \leftrightarrow \frac{1}{t_B^l}. \quad (3.5a-d)$$

The physics of equation (3.5a) is clear:  $c^*k_B T \leftrightarrow G$  merely expressed the fact that the small strain shear modulus of a Gaussian network is  $c^*k_B T$ . The physical meanings of the rest of the associations can be understood by considering a small strain uniaxial tension test, where  $\lambda - 1 \equiv \epsilon \ll 1$ . For this case, equations (3.2) and (3.4) reduce to (see electronic supplementary material)

$$\sigma_{11} = \underbrace{3c^*k_B T \left\{ \frac{c_p}{c^*} \epsilon + \sum_{l=1}^M \frac{c_l}{c^*} \int_0^t e^{-k_d^l(t-\tau)} \frac{d\epsilon}{d\tau} d\tau \right\}}_{\text{equation (3.2)}} \leftrightarrow 3G \underbrace{\left\{ \rho_p \epsilon + \sum_{l=1}^M \bar{\gamma}_\infty^l t_B^l \int_0^t e^{-(t-\tau)/t_B^l} \frac{d\epsilon}{d\tau} d\tau \right\}}_{\text{equation (3.4)}}. \quad (3.5)$$

The term on the right-hand side of equation (3.5) is the generalized Maxwell model in linear viscoelasticity, with relaxation modulus  $Y(t)$  given by the Prony series:

$$Y(t) = E_\infty + (E_0 - E_\infty) \sum_{l=1}^M a_l e^{-t/t_l}, \quad \sum_{l=1}^M a_l = 1 \quad (3.6a)$$

where

$$E_\infty = 3G\rho_p = 3c_p k_B T, \quad E_0 = 3G, \quad (3.6b)$$

are the plateau and instantaneous Young's modulus, respectively. In addition, the concentrations, the kinetic coefficients, healing rates and breaking time constants can be identified with relaxation times by

$$a_l = \frac{3G\bar{\gamma}_\infty^l t_B^l}{E_0 - E_\infty} = \frac{\bar{\gamma}_\infty^l t_B^l}{1 - \rho} = \frac{c_l}{c^*}, \quad \rho_p = \frac{c_p}{c^*}, \quad k_d^l = 1/t_B^l \quad (3.6c)$$

This proves the equivalence of the two models if linear breaking kinetics is assumed.

## (b) Nonlinear chain kinetics

As commonly observed [11] and is also the case for PVA gel, a power-law model of the form given by equation (2.6) fits the data with fewer material parameters (see the experimental section). Indeed, in the limit of small strains, it has been shown that equation (2.12b) reduces to a linear viscoelastic model with tensile relaxation function given by the power-law form [4]:

$$Y(t) = 3G[\rho + n(t)] = 3G\rho + \frac{3G\bar{\gamma}_\infty t_B}{2 - \alpha_B} [1 + (\alpha_B - 1)t/t_B]^{(2-\alpha_B)/(1-\alpha_B)}. \quad (3.6)$$

The exponent  $(2 - \alpha_B)/(1 - \alpha_B)$  shows here that the material parameter  $\alpha_B$  controls the relaxation spectrum. Physically, due to different lengths of chains between physical cross-links, one expects a distribution of relaxation modes in the dual cross-link network PVA network. For the case of  $\alpha_B = 1$ , only one such relaxation mode is considered. We note that with a small modification, one can extend the Eulerian formulation to include more complex breaking kinetics. First, it can be shown that equation (3.2) can be rewritten as (see electronic supplementary material)

$$\sigma = c^*k_B T \left\{ \frac{c_p}{c^*} (F(t)F^T(t) - I) - F(t) \left[ \sum_{l=1}^M \frac{c_l}{c^*} \int_0^t e^{-k_d^l(t-\tau)} \frac{d}{d\tau} [F^{-1}(\tau)F^{-T}(\tau)] d\tau \right] F^T(t) \right\} - pI. \quad (3.7)$$

As is well known, any linear viscoelastic solid with tensile relaxation function  $Y(t)$ , can be decomposed into its spectral density  $H$  [12]

$$Y(t) - E_\infty = \int_0^\infty H(u)e^{-t/u} du \Rightarrow Y(t) - E_\infty = \lim_{M \rightarrow \infty} \sum_{l=1}^M H(u_l)e^{-t/u_l} \Delta u_l. \quad (3.8)$$

For example, a generalized Maxwell solid has a discrete spectrum since  $H$  is a sum of Dirac delta functions  $\delta_{\text{dirac}}$ , i.e.  $H(u) = 3c^*k_B T \sum_{l=1}^M (c_l/c^*)\delta_{\text{dirac}}(u - t_B^l)$ . Hence an extension of equation (3.7) is

$$\boldsymbol{\sigma} = c^*k_B T \left\{ \frac{c_p}{c^*} (\mathbf{F}(t)\mathbf{F}^T(t) - \mathbf{I}) - \mathbf{F}(t) \left[ \int_0^t \left( \int_0^\infty H(u)e^{-t/u} du \right) \frac{d}{d\tau} [\mathbf{F}^{-1}(\tau)\mathbf{F}^{-T}(\tau)] d\tau \right] \mathbf{F}^T(t) \right\} - p\mathbf{I}. \quad (3.9)$$

Equations (2.21) and (3.9) would, therefore, allow us to determine the distribution tensor  $\boldsymbol{\mu}$  in the TNT for a more general class of kinetic models. More importantly, it shows that the linear kinetic model can be used to approximate any viscoelastic behaviour. The key is that the coefficients in the linear kinetic model can be found from spectral analysis. For example, for PVA gel, the relaxation function  $Y$  for small strains is given by [13]

$$Y(t) = 3G\rho + 3G \frac{\bar{\gamma}_\infty t_B}{2 - \alpha_B} (1 + (\alpha_B - 1)t/t_B)^{1-[1/(\alpha_B-1)]}. \quad (3.10)$$

The spectral density  $H$  for the power-law model equation (3.10) is (see electronic supplementary material)

$$H(u) = \frac{3G\bar{\gamma}_\infty t_B}{2 - \alpha_B} \left( \frac{t_B}{\alpha_B - 1} \right)^\lambda \frac{u^{-\lambda-1} e^{-(t_B/(\alpha_B-1))u^{-1}}}{\Gamma(\lambda)}, \quad \lambda = \frac{2 - \alpha_B}{\alpha_B - 1}. \quad (3.11)$$

This information allows one to select a finite number of terms in the Prony series to accurately represent the material behaviour in a fixed time interval, as we shall demonstrate below by comparing both theories with experiments.

## (c) Experimental comparison

### (i) Material preparation

Since synthesis details have been covered in previous works [13,14] we briefly summarize the procedure here. The first step is to make the chemically cross-linked gel by mixing a glutaraldehyde solution into a PVA solution at pH = 1.4 adjusted by hydrochloric acid. The PVA concentration in the solution was 12% and the molar ratio of chemical cross-linker and PVA monomers was 1 : 500. The solution was then injected into a mould. After 24 hours, the chemically cross-linked gel was removed from the mould and washed with water to neutralize the pH. Then the chemical gel was soaked in a NaCl/Borax solution (Borax, 1 mM $l^{-1}$ ; NaCl 90 mM $l^{-1}$ ) for 3–4 days allowing the formation of dynamic ionic bonds. Once the NaCl/Borax soak was completed, the samples were ready to be used in experiments.

### (ii) Mechanical testing

Uniaxial tension tests were performed using a custom-built tensile tester; [15] Zaber X-LSM200A-E03 translation stage was used to position the sample. The stage was controlled by Zaber console software. Force was measured using an Interface SMT 1–1.1 load cell, with a capacity of 1.1 lbf (about 4.9N). Displacement was measured using an OMEGA LD620 linear variable displacement transducer. The force and the displacement signals were recorded by a Keithley Model 2701 multiplexing digital voltmeter every 0.1 s. Samples were cut into strips 2 mm thick, 10 mm wide

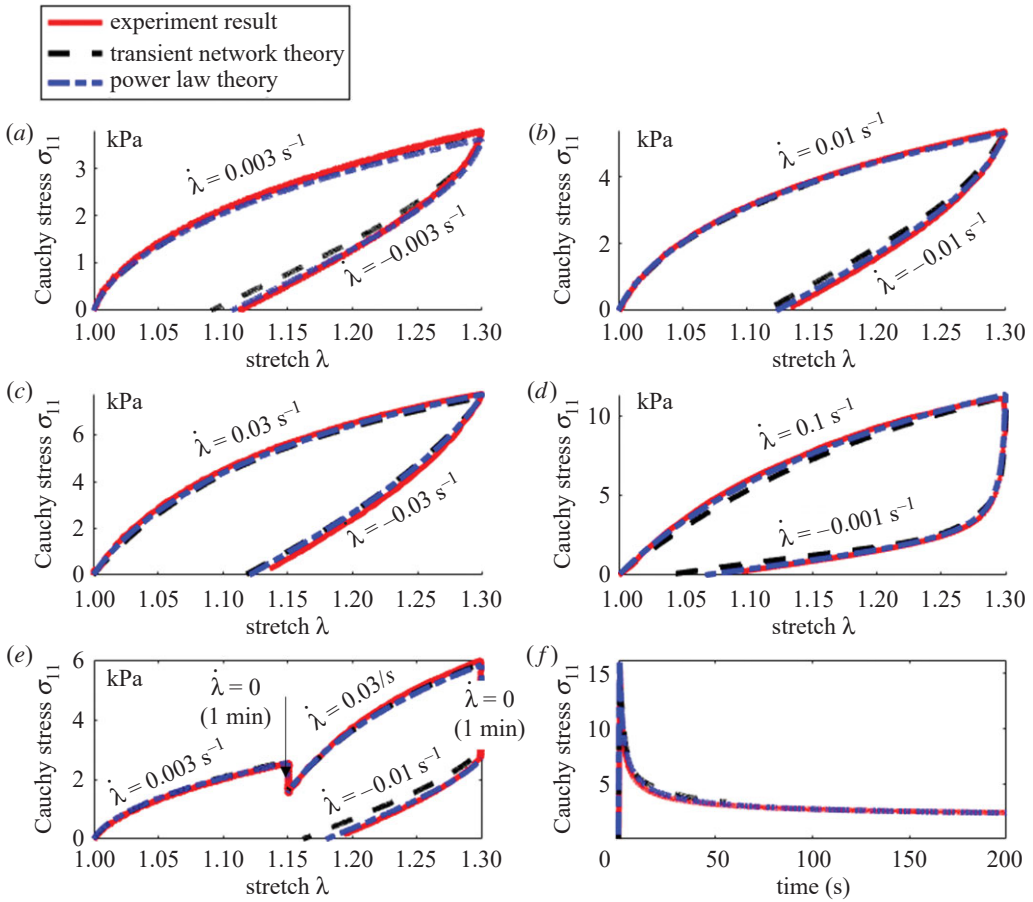


**Figure 5.** Comparison of experiments with the transient network (Eulerian) and Lagrangian approach. Stress is measured in kPa and time in seconds. The TNT assumes linear kinetics with one permanent network and two transient networks ( $M = 2$  in equation (3.12b)). The Lagrangian approach uses the power-law model equation (3.12a). The parameters used to simulate experiments are given in table 1. (Online version in colour).

and clamped between a pair of sandpaper-lined aluminium grips separated by a gauge length of approximately 30 mm. All tests were performed in mineral oil to prevent drying.

Tests were performed sequentially using the same sample for consistency of results. Between each test, the sample is rested for at least 12 min to fully recover to its original state. We performed three types of tests. We first carried out three cyclic tests where the sample were loaded to a stretch of 1.3 at stretch rates of  $\dot{\lambda} = 0.003 \text{ s}^{-1}$ ,  $0.01 \text{ s}^{-1}$ ,  $0.03 \text{ s}^{-1}$  (figure 5a–c). This is followed by unloading to a stretch ratio of 1 at the same rate. We next considered a situation where the sample was loaded to  $\lambda = 1.3$  at  $\dot{\lambda} = 0.1 \text{ s}^{-1}$  and unloaded to  $\lambda = 1$  at  $\dot{\lambda} = 0.001 \text{ s}^{-1}$  (figure 5d). We then carried out a complex loading history in which the sample was loaded to a stretch of  $\lambda = 1.15$  at a rate of  $\dot{\lambda} = 0.003 \text{ s}^{-1}$ , held for 1 min and then loaded to  $\lambda = 1.3$  at  $\dot{\lambda} = 0.03 \text{ s}^{-1}$ , held for another 1 min and then unloaded at a rate of  $\dot{\lambda} = 0.01 \text{ s}^{-1}$  (figure 5e). Finally, a relaxation test at a maximum stretch of 1.3 is carried out with an initial stretch rate of  $\dot{\lambda} = 0.5 \text{ s}^{-1}$  (figure 5f).

The nominal stress  $S$  (force in load cell divided by initial cross-section area of sample) versus stretch ratio for different tests is plotted in figure 5. Specializing (2.11b) and (2.22) to uniaxial tension, the nominal stresses  $S$  are, respectively:

$$S = G \left\{ (\rho_p + \bar{n}(t)) \left[ \lambda(t) - \frac{1}{\lambda^2(t)} \right] + \bar{\gamma}_\infty \int_0^t \phi_B(t - \tau) \left[ \frac{\lambda(t)}{\lambda^2(\tau)} - \frac{\lambda(\tau)}{\lambda^2(t)} \right] d\tau \right\} \quad (3.12a)$$

**Table 1.** Model parameters used to simulate experiments.  $\alpha_B$  is dimensionless.

power-law model (Lagrangian)	$G\rho$ (kPa)	$G\gamma_\infty$ (kPa.s <sup>-1</sup> )	$\alpha_B$	$t_B$ (s)	
	2.347	19.91	1.634	0.4618	
transient network linear kinetics (Eulerian)	$c_0kT$ (kPa)	$c_1kT$ (kPa)	$k_d^1$ (s <sup>-1</sup> )	$c_2kT$ (kPa)	$k_d^2$ (s <sup>-1</sup> )
	4	26	0.4	10	0.04

and

$$S = c^*k_B T \left\{ \left( \frac{c_p}{c^*} + \sum_{l=1}^M \frac{c_l^*}{c^*} e^{-k_d^l t} \right) \left[ \lambda(t) - \frac{1}{\lambda^2(t)} \right] + \sum_{l=1}^M \frac{c_l^*}{c^*} \int_0^t k_d^l e^{-k_d^l(t-\tau)} \left[ \frac{\lambda(t)}{\lambda^2(\tau)} - \frac{\lambda(\tau)}{\lambda^2(t)} \right] d\tau \right\}, \quad (3.12b)$$

where  $\phi_B$  and  $\bar{n}(t)$  in equation (3.12a) are given by equations (2.4) and (2.7). In the continuum description equation (3.12a) four parameters are needed to completely specify the constitutive model. These are:  $G\rho_p$ ,  $G\gamma_\infty$ ,  $\alpha_B$  and  $t_B$ . Procedures of determining these parameters have been thoroughly discussed in several papers [5,12] and will not be repeated here. The parameters used to simulate experiments are listed in table 1. In the statistical mechanics approach based on linear kinetics, the number of parameters needed to determine the constitutive behaviour is  $2M + 1$ . Specifically, they are  $c_p$ ,  $k_d^l$ ,  $c_l^*$ . In the comparison below, the number of networks,  $M$ , used is 2, so the number of material parameters is 5. Parameters for both models are listed in table 1.

Figure 5 shows excellent agreement between models and experiment. Given the variety of loading histories, the agreement between theory and experiments is striking and demonstrates the efficacy of both approaches. The discrepancy between transient network prediction and experiments is slightly larger than the power-law model. However, this can be readily remedied by using optimization techniques for the fitting or including additional transient networks (increasing  $M$ ). On a final note, the observed agreement between theory and experiment is for intermediate and low stretch rates. However, as noted in [4], equation (3.12a) starts to break down at high stretch rates. Specifically, at stretch rates  $\dot{\lambda} = 0.9 \text{ s}^{-1}$ , equation (3.12a) underpredicts the stress. At high rates, it is likely that some physical bonds act like permanent bonds, so the behaviour of the gel is more solid-like. Since the Eulerian approach (with a sufficiently large  $M$  or number of subnetworks) is equivalent to the Lagrangian approach, we also expected it to break down at these high strain rates.

## 4. Discussion

We discussed two complementary approaches to model soft material viscoelasticity. We have demonstrated that both approaches agree well with uniaxial tension tests on a PVA viscoelastic hydrogel.

- The Lagrangian viewpoint, which is consistent with the idea of a viscoelastic solid, is based on a well-defined reference configuration about which the network deformation can be defined. This model, therefore, defines the deformation of a population in the network by the total deformation gradient  $F$ , and the deformation gradient  $F_{\tau \rightarrow t}$  of the network at the time they were born.
- The Eulerian viewpoint, which is consistent with the idea of an elastic fluid, does not rely on the existence of a reference configuration. Instead, it describes the network in terms of the distribution of the stretch of each of its chains, which through statistical averaging can provide an estimation of the mean network deformation via the conformation tensor  $\mu$ .

## (a) Incorporation of nonlinear viscoelastic mechanisms

Although the two classes of model discussed here were presented in their simplest version, their main advantage is a deep connection with the underlying physics of the networks. Two additional sources of nonlinearity can be added to these models.

- (a) *Elastic nonlinearity*: First, there is the nonlinearity due to strain stiffening of the chains, as the neo-Hookean model, which is based on Gaussian statistics, is limited to small to moderately large strains. This effect can be accounted for by using a different strain energy function. In the Lagrangian approach, strain stiffening effects are already included since equation (2.5b) is valid for any hyper-elastic strain energy density. In the TNT, this effect can, for instance, be accounted for by using a Langevin chain model to capture the limit stretchability of flexible chains [16], or the compressive response of semi-flexible filaments [16,17]. However, for non-Gaussian chain models, one needs to use the full TNT model, which involves solving the partial differential equation (2.17) involving the chain distribution function  $\phi$  instead of equation (2.20).
- (b) *Coupling between chain elasticity and bond dynamics*: We have demonstrated both theoretically and experimentally that both approaches are identical when bond association dynamics is insensitive to deformation. This may not be the case for more complex materials, for example, polyampholyte gels are known to exhibit complex nonlinear viscoelastic behaviour that cannot be explained by a strain-independent bond dynamics model [18–20]. Hence there is a great need to study the coupling between mechanics and bond dynamics. The challenge for both approaches is to uncover bond dynamics models that correctly capture association/dissociation behaviour. In the Lagrangian approach, one can incorporate a phenomenologically based kinetic model for evolution of  $n(\tau; t)$  that accounts for coupling of association/dissociation with the deformation history. We have, recently, adapted this approach to quantify the viscoelastic behaviour of PA gels [21,22].

Coupling between stress and relaxation bond kinetics in the TNT framework can be explored by establishing a connection between the kinetic rate coefficient  $k_d$  and the chain tension. For example, in Eyring's theory [23,24], the rate of chain detachment is an exponential function of bond tension  $f$ :

$$k_d = k_d^0 \exp\left(\frac{f\delta}{k_B T}\right), \quad (4.1)$$

where  $k_d^0$  is the dissociation kinetic constant in the absence of force,  $\delta$  is a molecular distance that represents the force sensitivity of bond dissociation,  $k_B$  is the Boltzmann constant and  $T$  the absolute temperature (i.e. the bond becomes force-insensitive when  $\delta \rightarrow 0$ ). Since the force acting on a chain is a function of its end-to-end vector  $\mathbf{r}$ ,  $k_d$  is a function of  $\mathbf{r}$  in the general formulation [25], hence the full TNT model has to be used and it is necessary to solve a partial differential equation involving the chain distribution function  $\phi$ , e.g. equation (2.17), as well as a differential equation that governs the time chain concentration. Once this is done, the true stress can be determined using equation (2.18).

## (b) Comparative strengths and weaknesses of the Lagrangian and Eulerian approaches

We here discuss the strengths and limitations of each approach.

### (i) Lagrangian approach

The advantages of the Lagrangian approach are

- Flexibility of using any phenomenologically based strain energy density function  $W$  to describe network behaviour, although the association with chain statistics can be lost as a result.
- Relatively simple to incorporate phenomenologically based kinetic model for evolution of  $n(\tau; t)$  that accounts for coupling of association/dissociation with the deformation history.

The main disadvantage of the Lagrangian formulation are as follows:

- From a numerical viewpoint, it is necessary to keep track of a long history integral, whose size increases rapidly with simulation time. In finite-element calculations involving complex geometries, the simulation time can be prohibitively long.
- The direct connection with chain statistics is lost since phenomenological models for strain energy density and bond association/disassociation are used.

### (ii) Eulerian approach: full TNT

Assessment of the Eulerian approach depends on its level of refinement. There are two different versions of this approach, denoted here as the (full) TNT and the scaled down RTNT, each with distinct advantages and inconvenience. We, therefore, discuss them separately. The TNT relies on a full description of the chain distribution  $\phi$ , its evolution equation via a Fokker–Planck differential equation and associated differential equations describing evolution of chain concentrations. The solution of these equations determines the network stress, stored elastic energy and energy dissipation. This formulation, therefore, provides a detailed description of the full chain distribution over time, with the following advantages:

- It is not necessary to know the network's history, but rather its physical state (through the chain distribution function) that evolves over time.
- Originates from the behaviour at the chain level and can be adapted for non-affine deformation [7,26].
- It naturally incorporates nonlinear molecular details such as chain stiffening, force-dependent bond dynamics [25] and chain damage [27].

Because it possesses a high level of microstructural detail, the TNT is, however, limited by the following shortcomings:

- The solution of the Fokker–Planck equation (equation (2.16)) that determines the evolution of the distribution requires the implementation of a numerical solution over the full chain configuration space. For a macroscopic problem, this procedure needs to be repeated for each material point (or Gauss quadrature points in a finite-element implementation), necessitating significant computational resources.
- The evaluation of continuum-scale quantities, such as the true stress, the stored elastic energy or the rate of dissipation require integration over the full chain configuration space. This again can be prohibitively expensive for practical, macroscopic problems. This difficulty can be overcome by developing semi-analytical models.

### (iii) Eulerian approach: reduced TNT

The reduced TNT provides a description of the network in terms of the conformation tensor (i.e. the covariance of the distribution  $\phi$ ). This model reduction bypasses the computational cost of the TNT, while preserving most of its structure. It, therefore, has the following strengths:

- It is not necessary to know the network's history, but rather its physical state (now through the conformation tensor) that evolves over time.

- The evolution of the conformation tensor does not require the solution of a *spatial* differential equation [28]. Instead, its update follows a simple evolution equation (shown in equation (2.20)).
- The true stress stored elastic energy and dissipation can all be directly recovered from the knowledge of the conformation tensor (as seen in equation (2.22c) for the stress).

Because it is a reduced model, this approach suffers from the following limitations:

- Less flexibility on the choice of chain statistics. For example, the Gaussian chain model may not be able to fully capture stress–strain behaviour in experiments.
- While it is possible to incorporate the effect of nonlinear effects, such as chain stiffening and nonlinear chain dynamics, such models rely on macroscopic assumptions or mean-field approximations, as discussed in [16].

Finally, one of the advantages of both approaches is their ability to predict the local dissipation rate. Indeed, a difficulty inherent in linear viscoelastic theory is that it does not address the amount of internal dissipation. For example, given the relaxation function, classical viscoelastic theory allows one to uniquely determine the tension in a viscoelastic bar during a constant strain rate test. However, one cannot determine the amount of energy dissipated until the bar is returned to its initial stress-free state—e.g. by specifying the unloading history. This weakness of classical theory makes it difficult to analyse the size of the dissipation zone in the fracture of viscoelastic solids.

### (c) Open questions and opportunities

To conclude our discussion, we list here a number of open questions and challenges when it comes to accurately describing the physical behaviour of dynamic and viscoelastic polymers. In this context, some of the most obvious challenges are related to the onset of damage, fracture and adhesion of these materials, but also in being able to accurately capture the deformation mechanisms in polymer with more complex structures and bond dynamics.

#### (i) Fracture and adhesion

A fundamental but unsolved problem in fracture and adhesion is determining the energy dissipation during crack growth from basic principles. The standard approach is to assume a rate-independent local failure process that is confined to a single plane of molecular dimension [29,30]. In this approach, a line cohesive zone is used to model the local failure process (e.g. chain scission in elastomers) and to introduce a fracture length scale. The material outside the cohesive zone is assumed to be linear viscoelastic. A slightly different approach was used by de Gennes [31], and Persson & Brener [32]. In their approach, the fracture length scale is determined by a critical stress criterion. The predictions based on these two approaches are very similar and a detailed comparison can be found in a recent work of Hui *et al.* [33]. However, there are many limitations associated with this standard approach. Briefly, these are:

1. Unlike the theories presented in this paper, classical linear viscoelastic theory does not provide the local dissipation rate, and this makes determination of the size of dissipation zone difficult, as noted, recently, by Hui *et al.* [33].
2. The standard fracture model assumes linear viscoelasticity and small deformation.
3. The assumption that the local fracture process is rate independent is valid only if the polymer is chemically cross-linked, it is not the case for soft materials with a mixture of physical and chemical cross-links.
4. Standard theory assumes that most of the fracture energy is dissipated by viscoelasticity: the amount of energy dissipated by the local failure process is a very small fraction of the fracture energy.

5. Standard theory assumes no significant coupling between local failure process and continuum solutions.

Assumptions (3–5) are violated even for simple networks. Indeed, Slotman *et al.* [34] have shown that, even for simple elastomeric networks, chain scission is not confined to a single molecular plane directly ahead of the crack tip, instead, it is delocalized in a damage zone surrounding the crack tip, the size of which can be hundreds of micrometres. In addition, the energy dissipated by chain scission can be a significant fraction of the total dissipated energy. Finally, because the size of damage zone in these experiments is sensitive to viscoelasticity (i.e. temperature and local stretch rate), it can increase by 100-fold depending on these factors. Taken together, these observations suggest that there is significant coupling between failure process and viscoelasticity.

The challenge is even greater for more complex networks that possess a combination of chemical and physical bonds. Here most of the dissipation comes from the breaking of the physical bonds. Dissipation and failure must be coupled since both chemical and physical bonds must break during crack growth. Recall that linear viscoelasticity has no effect on damage since the rate of dissociation of physical bonds is independent of strain. This is not the case for nonlinear viscoelasticity. Indeed, accelerated bond breaking due to stress concentration will give rise to a larger damage zone than that predicted by the Lake–Thomas mechanism for instance, which can have important consequences for redistribution of stress near the crack tip [35]. Accelerated bond breaking is also found to be an important factor in determining whether a crack will propagate, blunt or arrest in single dynamic networks [36]. Finally, the role of healing or bond association on fracture is not at all clear. The two models highlighted in this work, when properly extended, can account for these limitations. Moving in this direction, the TNT was, recently, used to describe rate-independent damage in elastic networks [27], suggesting that a generalized model that account for both irreversible damage from chain rupture and reversible bond dynamics can be developed.

## (ii) Characterizing the time-dependent mechanics of complex networks

Dynamic networks extend much beyond the realm of the flexible polymers discussed in this manuscript. A large variety of natural and synthetic soft materials consist of networks of molecular chains (from flexible to athermal) cross-linked by dynamic bonds. We here provide a non-exhaustive list of materials for which the relationship between structure, dynamics and mechanical response could potentially be explored with the discussed methodologies.

*Biological and other complex dynamic networks.* Almost all soft animal tissues [37] but also plant [38] and fungi [39] display dynamic responses as required for growth, self-repair and adaptation. In contrast to flexible polymers, the cytoskeleton and biological tissues are typically made of a complex network that contain semi-flexible filaments, which can make up aligned, anisotropic networks (figure 6a). Connections between these filaments can be made of a variety of dynamic bonds that can be active (such as acto-myosin connections), increase their lifetime with force (as described by catch bonds [40]), or simply be mediated by enzymes [41]. As a consequence, these networks display very complex viscoelastic properties and can modify their architecture and anisotropy over time [42]. A typical example is the realignment of collagen fibres with stretch over long-time scales, or the reorganization of the tissue architecture by cells [43]. Because bond dynamics is often mediated by biological processes, the physical model presented here can provide a natural bridge between the mechanics, reorganization and biological processes.

*Hydrogels.* Perhaps among of the most studied class of soft biomaterials are hydrogels derived from biological components as in agarose, alginate or collagen gels. In these systems, molecular bonds are often heterogeneously distributed and form clusters, thereby affecting the network relaxation dynamics. This gives rise to rich and nonlinear viscoelastic behaviours that may be challenging to capture with phenomenological models. For instance, alginate gels are traditionally formed from high molecular weight alginate that is cross-linked with divalent cations (e.g.  $\text{Ca}^{2+}$ ),

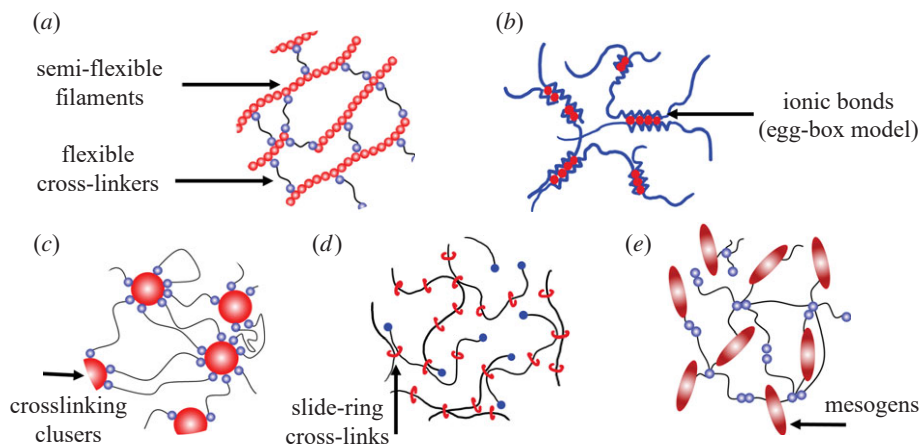


**Figure 6.** Schematics of complex dynamic polymer networks whose mechanical response could be described by the physically motivated approaches described in this work. (a) Biological networks often consist of semi-flexible polymer filaments cross-linked via flexible polymer by bonds that can be reversible. (b) Biopolymers, such as alginates, consist of ionic connections organized in substructural units (egg-box). (c) Similarly, polymer nanocomposites use nanoparticles (such as nano clay) to create stable clusters of transient bonds. (d) Dynamic cross-links can be replaced by sliding connections in viscoelastic gels, made of polyrotaxane for instance. (e) Finally, a transient flexible network can be decorated by high aspect ratio macromolecular units to create transient liquid crystal elastomers. (Online version in colour.)

which has been described by the egg-box model [44] (figure 6*b*). The relaxation behaviour is stress-dependent, behaving exclusively elastic under small loads but displaying faster and faster relaxation dynamics as the load increases. Such stress-dependent bond dynamics, also exhibited by nanocomposite gels (figure 6*c*), could be naturally integrated in the physically motivated model discussed in this work (figure 6).

*Slide-ring gels* (figure 6*d*): These networks constitute a new class of hydrogels where polymer chains are threaded by slide rings (typically made of rotaxane and cyclodextrin molecules), which, when cross-linked produce sliding junctions [45]. Thus, as opposed to detaching and reattaching over time, the cross-links are able to slide along the chains until they hit an end-cap, after which the material becomes elastic again. This pulley-effect [46] gives slide-ring gels unique tensile properties that combine nonlinear elasticity and a viscous component that can be tuned via the gel design. The physically motivated models presented here provide an interesting direction to couple molecular mechanisms such as ring entropy, chain entropy and the dynamics of ring sliding. In this context, it has, recently, been shown that the TNT [47] could naturally be adapted to describe the sliding process, in a way that is analogous to bond dynamics.

*Transient liquid crystal elastomers* (figure 6*e*): Liquid crystal elastomers are made of hybrid networks of flexible chains and unidirectional molecular units (the mesogens) whose alignment is coupled with the chain deformation. This coupling gives rise to several interesting effects such as mechanical actuation and soft elasticity [48]. Actuation originates from a first-order transition of the aligned (or nematic phase) to an isotropic phase of the mesogens, thereby producing a significant contraction in the direction of alignment. By contrast, the phenomenon of soft elasticity arises in the nematic phase, where the coupling between mesogen rotation and chain deformation leads to a low to negligible energy mode during shear deformation. While the fabrication of a single-crystal LCE has proved challenging, new generations of LCE with dynamic bond now offers new opportunities [49]. A wide variety of structures can be created (i.e. main chain or side chain LCE), with various mesogen geometry and network connectivities. Similarly, the bond dynamics may arise from a variety of chemistries [49] and can be enabled from external stimuli that range from temperature, light or the presence of a catalyst. Like flexible networks, transient LCEs exhibit stress relaxation and creep, but these processes are coupled with mesogen rotation

and realignment, which significantly increase the complexity of the response [49]. The physically motivated models discussed here could provide a good starting point to consider bond dynamics, mesogen deformation and chain deformation. For instance, the RTNT has, recently, been extended to the consideration of anisotropic networks made of stiff rods that are transiently cross-linked by flexible chains [50] and could capture the effect of deformation rate on rod alignment and network anisotropy. Additional research efforts are needed to describe soft elasticity and contraction when bond dynamics is activated.

## 5. Summary

To summarize, we have presented here two different, yet complementary physically based continuum formulations to describe the time-dependent mechanical behaviour of polymer networks with dynamic cross-links. We have shown that the key difference between these formulations stems from the point of view of the modellers when describing the kinematics of flexible chains within the space of conformations. When the viewpoint is Lagrangian, the model relies on the existence of a reference state, which is updated over time as chains dissociate and associate with the network over time. Mathematically, this yields an (time-) integral formulation where elastic energy and stresses are explicitly written in terms of the deformation's history. When the viewpoint is Eulerian, the physical state of a material point is entirely described by the statistical distribution of its effective chains (and does not rely on a reference state). The effects of deformation, chain dissociation and association on this distribution is then captured by a spatio-temporal differential equation (the Fokker–Planck equation), which can subsequently be used to evaluate the elastic energy and stress in the network. We have further shown that this formulation can be greatly reduced when chains are linear and bond reaction kinetics remain independent from deformation.

For simple networks, we found that these two models converge to the same solution, thereby confirming that they can be considered as dual mathematical formulations (integral and differential) englobing the same physical principles. Yet, they each possess their own advantages and drawbacks when it comes to deriving analytical and numerical solutions to describe more complex networks. We conclude that such physically informed models can potentially bridge the gap between the molecular, supramolecular and continuum scales. While they are still in their infancy, they are, therefore, likely to become important tools to better understand complex deformation mechanisms during damage, fracture and within complex supramolecular assemblies.

**Data accessibility.** The manuscript contains experimental data that have been archived in eCommons, and can be accessed at the following repository: Zehnder, Alan; Cui, Fan; Hui, Chung-Yuen; Vernerey, Franck, “Physically-motivated models of polymer networks with dynamic cross-links: comparative study and future outlook,” dataset: <https://hdl.handle.net/1813/110218>, October 2021.

**Authors' contributions.** F.J.V. and C.Y.-H. conceived the study, designed the study, coordinated the study and drafted the manuscript. F.C. and A.Z. collected laboratory data and contributed to the writing and editing of the manuscript. All authors gave final approval for publication and agree to be held accountable for the work performed therein.

**Competing interests.** We declare we have no competing interests.

**Funding.** F.J.V. gratefully acknowledges the support of the National Science Foundation under award no. 1761918. C.Y.-H. and A.Z. are supported by the National Science Foundation, USA under grant no. CMMI-1903308.

**Acknowledgements.** The content is solely the responsibility of the authors and does not necessarily represent the official views of the National Science Foundation.

## References

1. Taniguchi T, Urayama K. 2021 Linear dynamic viscoelasticity of dual cross-link poly(vinyl alcohol) hydrogel with determined borate ion concentration. *Gels* 7, 2. (doi:10.3390/gels7020071)

2. Mao Y, Lin S, Zhao X, Anand L. 2017 A large deformation viscoelastic model for double-network hydrogels. *J. Mech. Phys. Solids* **100**, 103–130. (doi:10.1016/j.jmps.2016.12.011)
3. Macosko C. 1994 *Rheology: principles, measurements, and applications*. Hoboken, NJ: Wiley.
4. Oldroyd JG, Wilson AH. 1950 On the formulation of rheological equations of state. *Phil. Trans. R. Soc. Lond. A* **200**, 523–541. (doi:10.1098/rspa.1950.0035)
5. Long R, Mayumi K, Creton C, Narita T, Hui C-Y. 2014 Time Dependent behavior of a dual cross-link self-healing gel: theory and experiments. *Macromolecules* **47**, 7243–7250. (doi:10.1021/ma501290h)
6. Guo J, Long R, Mayumi K, Hui C-Y. 2016 Mechanics of a Dual cross-link gel with dynamic bonds: steady state kinetics and large deformation effects. *Macromolecules* **49**, 3497–3507. (doi:10.1021/acs.macromol.6b00421)
7. Thien NP, Tanner RI. 1977 A new constitutive equation derived from network theory. *J. Non-Newtonian Fluid Mech.* **2**, 353–365. (doi:10.1016/0377-0257(77)80021-9)
8. Tanaka F, Edwards SF. 1992 Viscoelastic properties of physically crosslinked networks. *J. Non-Newtonian Fluid Mech.* **43**, 247–271. (doi:10.1016/0377-0257(92)80027-U)
9. Vernerey FJ, Long R, Brighenti R. 2017 A statistically-based continuum theory for polymers with transient networks. *J. Mech. Phys. Solids* **107**, 1–20. (doi:10.1016/j.jmps.2017.05.016)
10. Tanaka F, Edwards SF. 1992 Viscoelastic properties of physically crosslinked networks. 1. Transient network theory. *Macromolecules* **25**, 1516–1523. (doi:10.1021/ma00031a024)
11. Bonfanti A, Kaplan JL, Charras G, Kabla A. 2020 Fractional viscoelastic models for power-law materials. *Soft Matter* **16**, 6002–6020. (doi:10.1039/D0SM00354A)
12. Christensen R. 2012 *Theory of viscoelasticity: an introduction*. Amsterdam, The Netherlands: Elsevier.
13. Liu M, Guo J, Hui C-Y, Creton C, Narita T, Zehnder A. 2018 Time-temperature equivalence in a PVA dual cross-link self-healing hydrogel. *J. Rheol.* **62**, 991–1000. (doi:10.1122/1.5029466)
14. Mayumi K, Marcellan A, Ducouret G, Creton C, Narita T. 2013 Stress–strain relationship of highly stretchable dual cross-link gels: separability of strain and time effect. *ACS Macro Lett.* **2**, 1065–1068. (doi:10.1021/mz4005106)
15. Liu M, Guo J, Hui C-Y, Zehnder A. 2019 Crack tip stress based kinetic fracture model of a PVA dual-crosslink hydrogel. *Extreme Mech. Lett.* **29**, 100457. (doi:10.1016/j.eml.2019.100457)
16. Vernerey FJ. 2018 Transient response of nonlinear polymer networks: a kinetic theory. *J. Mech. Phys. Solids* **115**, 230–247. (doi:10.1016/j.jmps.2018.02.018)
17. Broedersz CP, MacKintosh FC. 2014 Modeling semiflexible polymer networks. *Rev. Mod. Phys.* **86**, 995–1036. (doi:10.1103/RevModPhys.86.995)
18. Meng F, Terentjev E. 2017 Theory of semiflexible filaments and networks. *Polymers* **9**, 52. (doi:10.3390/polym9020052)
19. Cui K, Ye YN, Sun TL, Chen L, Li X, Kurokawa T, Nakajima T, Nonoyama T, Gong JP. 2019 Effect of structure heterogeneity on mechanical performance of physical polyampholytes hydrogels. *Macromolecules* **52**, 7369–7378. (doi:10.1021/acs.macromol.9b01676)
20. Sun TL, Kurokawa T, Kuroda S, Ihsan AB, Akasaki T, Sato K, Haque MA, Nakajima T, Gong JP. 2013 Physical hydrogels composed of polyampholytes demonstrate high toughness and viscoelasticity. *Nat. Mater.* **12**, 932–937. (doi:10.1038/nmat3713)
21. Venkata SP, Cui K, Guo J, Zehnder AT, Gong JP, Hui C-Y. 2021 Constitutive modeling of bond breaking and healing kinetics of physical Polyampholyte (PA) gel. *Extreme Mech. Lett.* **43**, 101184. (doi:10.1016/j.eml.2021.101184)
22. Venkata SP, Cui K, Guo J, Zehnder AT, Gong JP, Hui C-Y. 2021 Constitutive modeling of strain-dependent bond breaking and healing kinetics of chemical polyampholyte (PA) gel. *Soft Matter* **17**, 4161–4169. (doi:10.1039/D1SM00110H)
23. Tobolsky A, Powell RE, Eyring H. 1943 *Chemistry of large molecules*. New York, NY: Interscience Publishers.
24. Chaudhury MK. 1999 Rate-dependent fracture at adhesive interface. *J. Phys. Chem. B* **103**, 6562–6566. (doi:10.1021/jp9906482)
25. Vernerey FJ, Shen T, Sridhar SL, Wagner RJ. 2018 How do fire ants control the rheology of their aggregations? A statistical mechanics approach. *J. R. Soc. Interface* **15**, 20180642. (doi:10.1098/rsif.2018.0642)
26. Mewis J, Denn MM. 1983 Constitutive equations based on the transient network concept. *J. Non-Newtonian Fluid Mech.* **12**, 69–83. (doi:10.1016/0377-0257(83)80005-6)
27. Vernerey FJ, Brighenti R, Long R, Shen T. 2018 Statistical damage mechanics of polymer networks. *Macromolecules* **51**, 6609–6622. (doi:10.1021/acs.macromol.8b01052)

28. Shen T, Long R, Vernerey F. 2018 Computational modeling of the large deformation and flow of viscoelastic polymers. *Comput. Mech.* **63**, 725–745. (doi:10.1007/s00466-018-1619-0)
29. Knauss WG. 1973 On the steady propagation of a crack in a viscoelastic sheet: experiments and analysis. In *Deformation and fracture of high polymers* (eds HH Kausch, JA Hassell, RI Jaffee), pp. 501–541. Boston, MA: Springer US.
30. Schapery RA. 1975 A theory of crack initiation and growth in viscoelastic media. *Int. J. Fract.* **11**, 141–159. (doi:10.1007/BF00034721)
31. de Gennes PG. 1996 Soft adhesives. *Langmuir* **12**, 4497–4500. (doi:10.1021/la950886y)
32. Persson BNJ, Brener EA. 2005 Crack propagation in viscoelastic solids. *Phys. Rev. E* **71**, 036123. (doi:10.1103/PhysRevE.71.036123)
33. Hui CY, Zhu B, Long R. Steady state crack growth in viscoelastic solids: comparative study and new insights on size of dissipation zone. *J. Mech. Phys. Solids*, submitted.
34. Slootman J, Waltz V, Yeh CJ, Baumann C, Göstl R, Comtet J, Creton C. 2020 Quantifying rate- and temperature-dependent molecular damage in elastomer fracture. *Phys. Rev. X* **10**, 041045. (doi:10.1103/physrevx.10.041045)
35. Guo J, Zehnder AT, Creton C, Hui C-Y. 2020 Time dependent fracture of soft materials: linear versus nonlinear viscoelasticity. *Soft Matter* **16**, 6163–6179. (doi:10.1039/D0SM00097C)
36. Shen T, Vernerey FJ. 2020 Rate-dependent fracture of transient networks. *J. Mech. Phys. Solids* **143**, 104028. (doi:10.1016/j.jmps.2020.104028)
37. Ambrosi D, Ben Amar M, Cyron CJ, DeSimone A, Goriely A, Humphrey JD, Kuhl E. 2019 Growth and remodelling of living tissues: perspectives, challenges and opportunities. *J. R. Soc. Interface* **16**, 20190233. (doi:10.1098/rsif.2019.0233)
38. Cosgrove DJ. 2005 Growth of the plant cell wall. *Nat. Rev. Mol. Cell Biol.* **6**, 850–861. (doi:10.1038/nrm1746)
39. Lalitha Sridhar S, Ortega JKE, Vernerey FJ. 2018 A statistical model of expansive growth in plant and fungal cells: the case of phycomyces. *Biophys. J.* **115**, 2428–2442. (doi:10.1016/j.bpj.2018.11.014)
40. Thomas WE, Vogel V, Sokurenko E. 2008 Biophysics of catch bonds. *Annu. Rev. Biophys.* **37**, 399–416. (doi:10.1146/annurev.biophys.37.032807.125804)
41. Ortega JKE. 2010 Plant cell growth in tissue. *Plant Physiol.* **154**, 1244–1253. (doi:10.1104/pp.110.162644)
42. Vernerey FJ, Akalp U. 2016 Role of catch bonds in actomyosin mechanics and cell mechanosensitivity. *Phys. Rev. E* **94**, 012403. (doi:10.1103/PhysRevE.94.012403)
43. Vernerey F, Sridhar S, Muralidharan A, Bryant S. 2021 Mechanics of 3D cell-hydrogel interactions: experiments, models, and mechanisms. *Chem. Rev.* **121**, 11085–11148.
44. Li L, Fang Y, Vreeker R, Appelqvist I, Mendes E. 2007 Reexamining the egg-box model in calcium–alginate gels with x-ray diffraction. *Biomacromolecules* **8**, 464–468. (doi:10.1021/bm060550a)
45. Ito K. 2012 Novel entropic elasticity of polymeric materials: why is slide-ring gel so soft? *Polym. J.* **44**, Art. no. 1. (doi:10.1038/pj.2011.131)
46. Mayumi K, Tezuka M, Bando A, Ito K. 2012 Mechanics of slide-ring gels: novel entropic elasticity of a topological network formed by ring and string. *Soft Matter* **8**, 8179–8183. (doi:10.1039/c2sm25508a)
47. Vernerey FJ, Lamont S. 2021 Transient mechanics of slide-ring networks: a continuum model. *J. Mech. Phys. Solids* **146**, 104212. (doi:10.1016/j.jmps.2020.104212)
48. Warner M, Terentjev EM. 2003 *Liquid crystal elastomers*. Oxford, UK: Oxford University Press.
49. Saed MO, Gablier A, Terentjev EM. 2021 ‘Exchangeable liquid crystalline elastomers and their applications. *Chem. Rev.* acs.chemrev.0c01057. (doi:10.1021/acs.chemrev.0c01057)
50. Lalitha Sridhar S, Vernerey FJ. 2020 Mechanics of transiently cross-linked nematic networks. *J. Mech. Phys. Solids* **141**, 104021. (doi:10.1016/j.jmps.2020.104021)